

Tuning of ZnO 1D nanostructures by atomic layer deposition and electrospinning for optical gas sensor applications

This content has been downloaded from IOPscience. Please scroll down to see the full text.

2015 Nanotechnology 26 105501

(<http://iopscience.iop.org/0957-4484/26/10/105501>)

View [the table of contents for this issue](#), or go to the [journal homepage](#) for more

Download details:

IP Address: 150.254.110.13

This content was downloaded on 19/02/2015 at 11:31

Please note that [terms and conditions apply](#).

Tuning of ZnO 1D nanostructures by atomic layer deposition and electrospinning for optical gas sensor applications

Roman Viter^{1,4}, Adib Abou Chaaya², Igor Iatsunskiy^{1,3},
Grzegorz Nowaczyk³, Kristaps Kovalevskis⁴, Donats Erts⁵, Philippe Miele²,
Valentyn Smyntyna¹ and Mikhael Bechelany^{2,6}

¹ Department of Experimental Physics, Odessa National I.I. Mechnikov University, 42, Pastera str., 65023 Odessa, Ukraine

² European Institute of Membranes (IEM, ENSCM-UM2-CNRS, UMR 5635), University of Montpellier 2, Place Eugène Bataillon, F-34095, Montpellier, France

³ NanoBioMedical Center, Uniwersytet im. Adama Mickiewicza w Poznaniu, 85 Umultowska str., 61-614, Poznan, Poland

⁴ Institute of Atomic Physics and Spectroscopy, University of Latvia, 19 Raina Blvd., LV 1586, Riga, Latvia

⁵ Institute of Chemical Physics, University of Latvia, 19 Raina Blvd., LV 1586, Riga, Latvia

E-mail: viter_r@mail.ru, adib.a.c@hotmail.com, yatsunskiy@gmail.com, nowag@amu.edu.pl, kristaps.kovalevskis@gmail.com, donats.erts@lu.lv, philippe.miele@univ-montp2.fr, smyntyna@onu.edu.ua and mikhael.bechelany@univ-montp2.fr

Received 9 November 2014, revised 13 January 2015

Accepted for publication 20 January 2015

Published 19 February 2015



CrossMark

Abstract

We explored for the first time the ability of a three-dimensional polyacrylonitrile/ZnO material—prepared by a combination of electrospinning and atomic layer deposition (ALD) as a new material with a large surface area—to enhance the performance of optical sensors for volatile organic compound (VOC) detection. The photoluminescence (PL) peak intensity of these one-dimensional nanostructures has been enhanced by a factor of 2000 compared to a flat Si substrate. In addition, a phase transition of the ZnO ALD coating from amorphous to crystalline has been observed due to the properties of a polyacrylonitrile nanofiber template: surface strain, roughness, and an increased number of nucleation sites in comparison with a flat Si substrate. The greatly improved PL performance of these nanostructured surfaces could produce exciting materials for implantation in VOC optical sensor applications.

 Online supplementary data available from stacks.iop.org/NANO/26/105501/mmedia

Keywords: atomic layer deposition, electrospinning, photoluminescence, ZnO, VOC, optical sensor, ethanol

(Some figures may appear in colour only in the online journal)

1. Introduction

ZnO is an n-type semiconductor with direct optical transitions and a band gap of 3.6 eV [1]. ZnO has been commonly used for different applications like optical coatings [2], light

emitting diodes [3], sensors [4], photovoltaics [5–7], and biosensors [8]. Recent approaches in nanotechnology allow one to fabricate ZnO nanostructures with high surface-to-volume aspect ratios, which is significantly important for sensor and biosensor applications.

There is of particular interest in the detection of volatile organic compounds (VOC) such as acetone and ethanol by

⁶ Author to whom any correspondence should be addressed.

means of metal oxide gas sensors. The traditional resistive gas sensors for ethanol detection operate at 120–450 °C [9]. Nanostructured metal oxides demonstrated reduced operating temperatures, from room temperature up to 250 °C [10, 11]. The nanostructured ZnO sensor managed to detect ethanol in 5–200 ppm at 200 °C [12]. Recently, optical gas sensors have attracted attention [9, 13, 14] because they are highly precise and can operate at room temperatures, which is sufficient to reduce power consumption. ZnO nanostructures have been successfully used for NO/NO_x and ammonia optical sensing. Detection was performed using the photoluminescence (PL) method [9, 13, 14]. Sensor calibration was obtained according to the change in PL intensity induced by adsorption of gas molecules [9, 13, 14]. However, the optical detection of VOCs like ethanol using ZnO nanostructures has not been reported yet.

Recently, we explored for the first time the ability of three-dimensional polyacrylonitrile/ZnO materials—prepared by a combination of electrospinning and atomic layer deposition (ALD) as a new material with a large surface area—to enhance the performance of ultraviolet (UV) photo-detection. The UV photoresponse current has been enhanced by a factor of 250 compared to that of a flat electrode [4]. ALD is a powerful technique for the deposition of metal oxide nanostructures [15]. We have reported on ALD deposition of ZnO nanostructures and their structural and optical properties [16, 17]. It was found that thin ZnO layers deposited on Si substrates showed no crystalline structure when their thickness was lower than 50 nm [17]. A methodology for tuning the optical and structural properties of ALD-deposited ZnO nanostructures was proposed [16]. Moreover, electrospinning is a good method for fabrication of one-dimensional (1D) semiconductor nanostructures [18] and organic nanofiber templates [4, 19–21]. The method is based on the polarization of precursors in a high-voltage electrostatic field and the elongation in one direction during deposition.

In this paper, ZnO 1D nanostructures (NSs) are tailored using the same techniques: ALD combined with electrospinning. Polyacrylonitrile fibers synthesized by electrospinning are used as a template for ZnO ALD deposition to enhance the specific surface of the ZnO 1D nanostructures. Structural, chemical, and optical properties of the obtained materials are investigated. It should be noted that the design of high-surface 1D ZnO NSs based on ALD deposition and electrospinning and the investigation of their optical properties for ethanol sensor applications has not been addressed yet.

2. Materials and methods

2.1. Materials

Polyacrylonitrile PAN ($M_w = 150\,000$) and dimethylformamide (ACS reagent, $\geq 99.8\%$) were purchased from Sigma Aldrich. Diethyl zinc (DEZ) ($Zn(CH_2CH_3)_2$, 95% purity, CAS: 557-20-0) was purchased from Sterm Chemical.

2.2. Electrospinning of PAN nanofibers

Polyacrylonitrile (10 wt% PAN) was dissolved in dimethylformamide (DMF). The electrospinning solution was maintained under agitation for 1 h and then heated in an oil bath at 80 °C for 10 min. The electrospinning machine we used was a homemade device using an HPx 600 605 generator (physical instruments) and a KDS 100 syringe pump [4, 19]. The polymer solution was electrospun in an ambient air atmosphere under an applied voltage of 25 kV with a flow rate of 3 mL h⁻¹ using a 0.7 mm diameter syringe connected to the positive output of the generator. A fix collector was placed 25 cm from the tip of the syringe and was related to the negative output of the generator. The droplet was transformed to a Taylor cone due to the electrostatic field applied between the syringe and the collector and then stretched to form a net of submicron fiber after the evaporation of the solvent.

2.3. ALD of ZnO

A homemade ALD setup [22, 23] was used to deposit ZnO thin layers on the electrospun nanofibers. ZnO was deposited at 100 °C using sequential exposures to DEZ and deionized water, separated by a purge with dry argon (flow rate of 100 sccm). The deposition protocol was as follows: (a) 2 s pulse of DEZ, 30 s exposure, and 50 s purge with dry Ar; (b) 3 s pulse of H₂O, 40 s of exposure, and 60 s purge with dry Ar. The selected pulse, exposure, and purge times were chosen both to ensure completion of the ALD surface reactions and to prevent mixing of the reactive species. The growth rate was typically 2 Å/cycle for ZnO [22, 23]. The growth per cycle was controlled by measuring the film's thickness on Si-wafer companion substrates placed in the reactor.

2.4. Structural and chemical characterization

Structural and chemical compositions of all 1D ZnO-based NSs were analyzed by scanning electron microscopy (SEM, S-4800, Hitachi), energy-dispersive x-ray (EDX) spectroscopy (SEM, S-4500, coupled with a Thermofisher EDX detector), and x-ray diffraction (XRD, PANalytical Xpert-PRO diffractometer equipped with a X'celerator detector using Ni-filtered Cu-radiation). From the latter, the grain size was calculated by the Debye-Scherrer equation. Transmission electron microscopy (TEM) images were obtained with a JEOL ARM 200F high-resolution transmission electron microscope (200 kV) with an EDX analyzer. Dark and bright field detectors were used.

2.5. Optical sensing

Optical properties of the samples were studied by PL spectroscopy. The PL of the samples was measured at room temperature using a homemade setup [16, 17]. The excitation of PL was performed with a solid-state laser (355 nm) and the emission spectra were recorded in the range of 360–800 nm [16, 17]. Gas-sensing measurements were performed in a homemade quartz chamber equipped with a gas inlet and

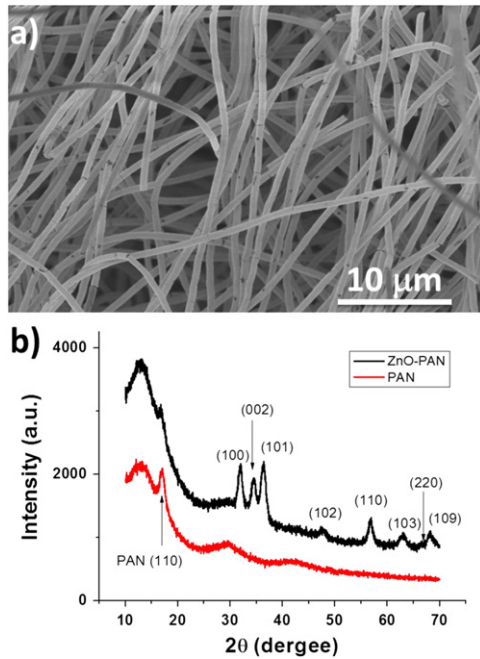


Figure 1. (a) SEM image of 1D ZnO NSs obtained with 300 s electrospinning time and coated with 50 cycles ALD ZnO at 100 °C. (b) XRD spectra of the obtained 1D NSs.

outlet valves. Ethanol vapors (150 ppm) were delivered into the chamber with an air flow. PL measurements of ZnO were performed after 5 min exposition in ethanol.

3. Results and discussion

Figure 1(a) shows the SEM image of 1D ZnO NSs obtained with 300 s of electrospinning time and coated with 50 cycles of ALD ZnO at 100 °C. The image indicates a conformal coating of the PAN nanofibers obtained by this method. EDX measurement (not reported here) has been performed on the sample to evaluate the chemical composition. The presence of Zn, O, N, and C can be observed. EDX confirms the stoichiometric composition of ZnO (Zn 49.3% and O 50.7%) of the sample.

XRD (figure 1) shows peaks at $2\theta = 31.74^\circ$, 34.42° , 36.22° , 47.53° , 56.61° , 62.86° , 68.03° , and 69.08° , respectively corresponding to (100), (002), (101), (102), (110), (103), (220), and (109) of the hexagonal wurtzite phase of ZnO, as generally observed with the ZnO thin films deposited by ALD [16, 17]. The average grain size, D , of the ZnO/PAN nanostructures was calculated using the Debye-Scherrer equation [16, 17]:

$$D = \frac{0.9 \cdot \lambda}{\beta \cdot \cos(\theta)} \quad (1)$$

where β , θ , and λ are full width of half maximum, diffraction angle, and x-ray wavelength ($\lambda = 0.154$ nm), respectively. The calculated value of the grain size was $D = 8.2 \pm 1.1$ nm. PAN nanofibers showed a characteristic XRD peak, related to the (110) reflection, centered at $2\theta \approx 17^\circ$, similar to what was

reported by Chen *et al* [24]. Deposition of an ALD layer over PAN nanofibers led to the shift of the XRD peak toward lower values of 2θ .

Figure 2 shows the TEM images at different magnifications of 1D ZnO NSs, obtained with 300 s of electrospinning time and coated with 50 cycles of ALD ZnO at 100 °C. The low-resolution TEM image in figure 2(a) confirms the conformal coating of the PAN nanofibers by ALD with a wall thickness of 20 nm ZnO. The growth rate was typically 2 Å/cycle for ZnO, as has been reported previously [22, 23].

An HRTEM image of the ZnO/PAN nanostructure is shown in figure 2(b). Using ImageJ software, the grain size distribution and the interplane distances for (100), (002), and (101) lattice planes were calculated, as shown in figure 2(c). The average grain size value was about 7.7 nm from the TEM data seen in figure 2(d), confirming the XRD results. The interplane distances for (100), (002), and (101) lattice planes 0.278, 0.25 and 0.24 nm, correspondingly, were lower than the interplane distances for ZnO, reported in the Joint Committee on Powder Diffraction Standards database. The decrease of the interplane distance could be due to strain effects resulting from the nanocrystalline size.

The PL spectra of electrospun PAN nanofibers and 1D ZnO NSs obtained with 300 s electrospinning time and coated with 50 cycles ALD ZnO at 100 °C are shown in figure 3. The PL spectrum of 1D ZnO/PAN NSs demonstrated two typical emission bands, located in the UV and visible regions and corresponding to near band emission (NBE) and deep level emission (DLE). It is worth noting that due to the high surface of PAN substrates, the intensity of ZnO/PAN emission was 2000 times higher than the same value for ALD 200 nm ZnO film deposited on a silicon substrate for both NBE and DLE (Supporting Information, SI2) [16, 17]. We note here that due to the low weight of the deposited PAN/ZnO 1D NSs, Brunauer–Emmett–Teller experiments could not be performed to quantitatively determine the specific surface area of the detectors.

Uncoated electrospun PAN nanofibers were also tested to have a blank spectrum for further comparative analysis. The obtained spectra were analyzed by Gaussian fitting using Origin 7 software. The determined peak positions are collected in table 1. Table 1 shows that the obtained peaks at 390–395 nm correspond to the NBE emission of ZnO. The peak at 403 nm corresponds to structural defects [16, 17]. Peaks at 423–428 nm could be related to Zn interstitials [16, 17], and peaks at 600–607 nm correspond to interstitial oxygen, as reported elsewhere [16, 17].

The most important question in this study relates to the mechanism of the amorphous-to-crystalline phase transition of ALD thin layers deposited on Si and on electrospun PAN nanofibers. 20 nm of ZnO deposited on a silicon substrate shows an amorphous nature [17], whereas 20 nm of ZnO deposited on PAN nanofibers shows a crystalline nature with an average grain size of 7.7 nm.

ZnO nanostructures were previously deposited on polymeric substrates [25, 26]. Li *et al* reported the deposition of ZnO on polyethylene-terephthalate (PET) [26]. The PET substrate was maintained under different stresses before ZnO

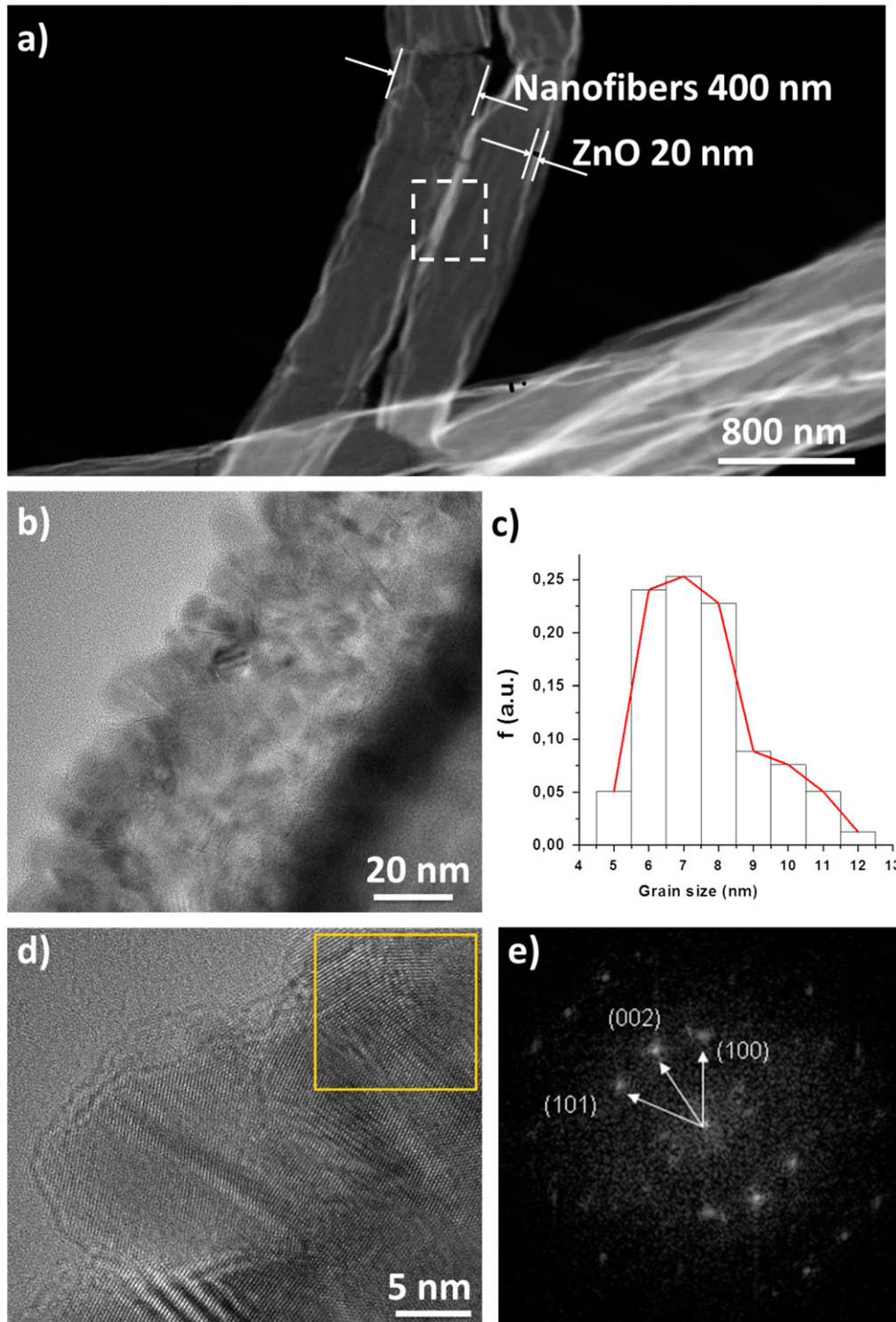


Figure 2. (a) TEM image of 1D ZnO NSs obtained with 300 s electrospinning time and coated with 50 cycles ALD ZnO at 100 °C. (b) High-resolution TEM (HRTEM) image of the area highlighted by the white square in (a). (c) Size distribution of ZnO nanoparticles. (d) HRTEM image of a ZnO nanoparticle. (e) Inverse fast Fourier transform of the area highlighted with a yellow square in the HRTEM image (d).

deposition. It was shown that the film thickness decreased and the crystalline quality of the films increased when a stress was applied to PET surfaces [26]. ALD of ZnO on polymeric substrates was also demonstrated by Heo *et al* [25]. Polyethersulfone (PES) substrates were treated with O₂ plasma. After the plasma treatment, the roughness of the substrates

increased proportionally to the time of the treatment. After ZnO deposition, XRD peaks for (100) and (002) ZnO reflections were detected. It was reported that PES roughness creates nucleation sites and stimulates growth perpendicular to the PES surface. The grain size decreased with the increase of the plasma treatment time.

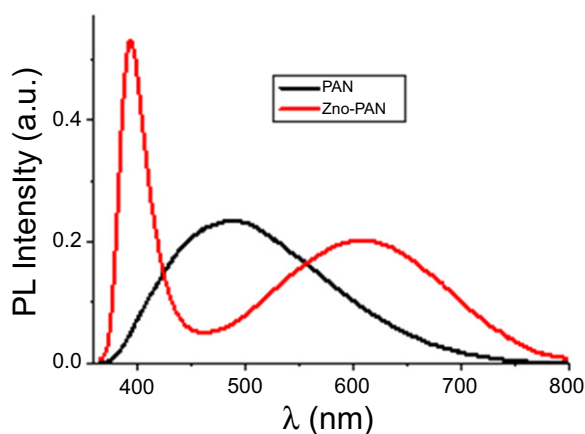


Figure 3. PL spectra of electrospun PAN nanofibers (black curve) and 1D ZnO NSs obtained with 300 s electrospinning time and coated with 50 cycles ALD ZnO at 100 °C (red curve).

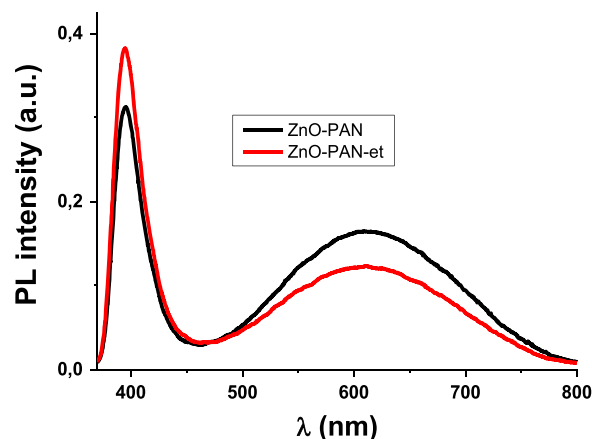


Figure 4. PL sensitivity test of ethanol vapor (150 ppm of ethanol) using 1D ZnO NSs obtained with 300 s electrospinning time and coated with 50 cycles ALD ZnO at 100 °C.

Table 1. PL peak positions of electrospun PAN nanofibers and 1D ZnO NSs obtained with 300 s electrospinning time and coated with 50 cycles ALD ZnO at 100 °C.

Sample	PL peak positions				
ZnO/PAN 1D NSs	390	403	423		607
PAN		433	485	557	

Li *et al* reported that ALD ZnO deposited over carbon nanotubes (CNTs) also grew crystalline nanorods [27]. It was reported that the surface defects of CNTs (such as bending in the nanotube, the finite size of crystalline domains, sp³-hybridized bonds, or functional groups created by oxidation) interact with ALD precursors and yield crystalline ZnO thin films [27]. ZnO growth on an organic polymer sublayer was also studied by Blumstengel *et al* [28]. The organic layers induced growth of ZnO crystallines of 5–10 nm grain size with different orientations. Two competitive growth processes were shown—lateral and vertical, in correspondence to the organic layer plane.

Thus, the ZnO growth over the organic templates is affected by the nucleation sites on the substrate surface [25, 26]. The nucleation sites are induced by the roughness, surface strain, surface defects, and impurities. The concentration of nucleation sites defines the grain size in the deposited ZnO nanolayers and their crystalline structures. As in the present work, a ZnO nanolayer was deposited on PAN nanofibers, according to the previously mentioned references, and the structural properties of PAN could define the structure of ALD-deposited ZnO nanolayers.

Heidari *et al* showed that electrospun PAN nanofibers had significant strain values [29]. Yu *et al* reported that PAN nanofibers' surface roughness depended on the nanofiber diameter: the smaller the diameter, the smoother the surface [30]. In the present work, the PAN nanofibers had an average diameter of 250–350 nm, which is a medium size according to Yu *et al* [30]. So the shift of the XRD peak of the PAN nanofibers toward lower values is related to the surface strain

relaxation in electrospun PAN nanofibers after ZnO deposition.

The amorphous-to-crystalline phase transition in ZnO nanolayers deposited on Si and PAN nanofiber substrates can be explained by the higher value of nucleation sites on PAN nanofiber surfaces and the surface strain of PAN nanofibers. There is still an open question related to the minimal thickness of the amorphous-to-crystalline phase transition in ZnO-PAN nanostructures, which will be a subject further investigation.

The prepared samples were tested to 150 ppm of ethanol. ZnO/PAN 1D nanostructures showed changes in PL intensity induced by ethanol adsorption (figure 4). It is known that ethanol is a donor-like gas to ZnO nanostructures [9–12]. It increases the conductivity of ZnO due to the electron transfer to its conduction band. In the present work, ethanol adsorption increased NBE and decreased DLE emission. Two possible mechanisms could induce these phenomena: (i) Ethanol was adsorbed on optical defects and passivated them, and (ii) surface-bend bending decreased due to the ethanol adsorption.

The calculated ratio of the integrated intensity of the NBE peak before and after ethanol exposure was 0.83 ± 0.04 , whereas the calculated ratio of the integrated intensity of the DLE peak before and after ethanol exposure was 1.31 ± 0.03 (Supporting Information, SI1). This means that the change of the sensor signal with 150 ppm of ethanol was approximately 20% and 30% for NBE and DLE, respectively. In comparison to the resistive ZnO ethanol sensors, these changes are much smaller, and additional sensor tests for a number of ethanol concentrations are needed. However, the presence of two peaks in the ZnO PL spectrum and their simultaneous changes due to the ethanol adsorption can make ZnO PL nanostructures suitable for recognition of different VOCs by analyzing the integrated parameters of the NBE and DLE peaks.

4. Conclusion

A novel concept of 1D ZnO/PAN nanostructures has been shown for optical sensor detection. The phase transition of ZnO ALD coating from amorphous to crystalline has been observed due to the properties of the PAN nanofiber template: the surface strain, the roughness, and the increased number of nucleation sites in comparison with the flat Si substrate. ZnO deposited on PAN NFs demonstrated a strong PL signal that compares to ZnO deposited on Si substrates. The response of ZnO/PAN 1D nanostructures to ethanol was not compatible with the resistive gas sensors, although the possibility of selective recognition of different VOCs is foreseen through ratio analysis of NBE and DLE peaks. We can conclude that the increase of the specific surface area of the electrode, which is provided by the network of the PAN NFs and the ALD conformal coating, is an efficient approach to improve the PL of ZnO nanostructures. The possibility of tuning the surface area, the band gap, and the chemical composition should allow the applications of these nanostructured electrodes in other fields, such as optical biosensing applications.

Acknowledgments

This work was partially supported by the EU under BIOSENSORS-AGRICULT, Contract PIRSES-GA-2012-318520 'Development of Nanotechnology-based Biosensors for Agriculture', 'Nanomaterials and their application to biomedicine' (contract number PBS1/A9/13/2012), and 'FOTONIKA-LV-FP7-REGPOT-CT-2011' (contract number 285912).

References

- [1] Bechelany M, Amin A, Brioude A, Cornu D and Miele P 2012 *J. Nanopart. Res.* **14** 980
- [2] Tonon C, Duvignacq C, Teyssedre G and Dinguirard M 2001 *J. Phys. D: Appl. Phys.* **34** 124
- [3] Chen M-J, Yang J-R and Shiojiri M 2012 *Semicond. Sci. Technol.* **27** 074005
- [4] Abou Chaaya A, Bechelany M, Balme S and Miele P 2014 *J. Mater. Chem. A* **2** 20650
- [5] Elias J, Bechelany M, Utke I, Erni R, Hosseini D, Michler J and Philippe L 2012 *Nano Energy* **1** 696
- [6] Elias J, Levy-Clement C, Bechelany M, Michler J, Wang G-Y, Wang Z and Philippe L 2010 *Adv. Mater.* **22** 1607
- [7] Elias J, Utke I, Yoon S, Bechelany M, Weidenkaff A, Michler J and Philippe L 2013 *Electrochim. Acta* **110** 387
- [8] Viter R et al 2014 *IEEE Sensors J.* **14** 2028
- [9] Sberveglieri G, Baratto C, Comini E, Faglia G, Ferroni A, Ponzoni A and Vomiero A 2007 *Sensors Actuators B* **121** 208
- [10] Chang S P 2012 *Nanotechnology and Advanced Materials* vol 486 ed G Yang p 39
- [11] Shao C, Chang Y and Long Y 2014 *Sensors Actuators B* **204** 666
- [12] Wang L, Kang Y, Liu X, Zhang S, Huang W and Wang S 2012 *Sensors Actuators B* **162** 237
- [13] Bismuto A, Lettieri S, Maddalena P, Baratto C, Comini E, Faglia G, Sberveglieri G and Zanotti L 2006 *J. Opt. A: Pure Appl. Opt.* **8** S585
- [14] Padilla-Rueda D, Vadillo J M and Laserna J J 2012 *Appl. Surf. Sci.* **259** 806
- [15] Marichy C, Bechelany M and Pinna N 2012 *Adv. Mater.* **24** 1017
- [16] Abou Chaaya A, Viter R, Baleviciute I, Bechelany M, Ramanavicius A, Gertner Z, Erts D, Smyntyna V and Miele P 2014 *J. Phys. Chem. C* **118** 3811
- [17] Abou Chaaya A, Viter R, Bechelany M, Alute Z, Erts D, Zaleskaya A, Kovalevskis K, Rouessac V, Smyntyna V and Miele P B 2013 *J. Nanotechnol* **4** 690
- [18] Dong X, Yang P and Shi R 2014 *Mater. Lett.* **135** 96
- [19] Selloum D, Abou Chaaya A, Bechelany M, Rouessac V, Miele P and Tingry S 2014 *J. Mater. Chem. A* **2** 2794
- [20] Nasr M, Chaaya A A, Bechelany M, Abboud N, Viter R, Eid C, Khoury A and Miele P 2015 *Superlattices Microstruct.* **77** 18
- [21] Khalil L, Eid C, Bechelany M, Abboud N, Khoury A and Miele P 2015 *Mater. Lett.* **140** 27
- [22] Abou Chaaya A et al 2013 *J. Phys. Chem. C* **117** 15306
- [23] Raghavan R, Bechelany M, Parlinska M, Frey D, Mook W M, Beyer A, Michler J and Utke I 2012 *Appl. Phys. Lett.* **100** 191912
- [24] Chen J, Li Z, Chao D, Zhang W and Wang C 2008 *Mater. Lett.* **62** 692
- [25] Heo J H, Ryu H and Lee W-J 2013 *J. Ind. Eng. Chem.* **19** 1638
- [26] Li T-C, Hsieh P-T and Lin J-F 2011 *Ceram. Int.* **37** 2467
- [27] Li X L, Li C, Zhang Y, Chu D P, Milne W I and Fan H J 2010 *Nano. Res. Lett.* **5** 1836
- [28] Blumstengel S, Kirmse H, Sparenberg M, Sadofev S, Polzer F and Henneberger F 2014 *J. Crystal Growth* **402** 187
- [29] Heidari I, Mashhadi M M and Faraji G 2013 *Chem. Phys. Lett.* **590** 231
- [30] Yu D-G, Zhou J, Chatterton N P, Li Y, Huang J and Wang X 2012 *Int. J. Nanomed.* **7** 5725